Desalination and Water Treatment
www.deswater.com

doi: 10.5004/dwt.2023.30192

316 (2023) 258–266
December

Fouling on aluminum-brass and titanium tube surface in environment of low-temperature multi-effect distillation for desalination

Shuhua Zhou[a], Tao Lu[a], Bing Ni[b,c,†], Shengqiang Shen[c], Xue Chen[a,*]

[a]*Beijing University of Chemical Technology, Beijing 100029, China, emails: xchen@buct.edu.cn (X. Chen), 2022400195@buct.edu.cn (S. Zhou), likesurge@sina.com (T. Lu)*
[b]*China ENFI Engineering Co., Ltd., Beijing 100038, China, email: 378459679@qq.com*
[c]*Dalian University of Technology, Dalian 116024, China, email: zzbshen@dlut.edu.cn*

Received 28 July 2023; Accepted 28 November 2023

ABSTRACT

Fouling on aluminum-brass tube and titanium tube in concentrated salt solutions are investigated with various calcium ion concentration and magnesium-to-calcium ion concentration ratio. The test tubes were placed in an environment with constant-temperature of 70°C and then the fouling depositions at different time points were accurately quantified throughout the 63-h process. Besides, the morphology and composition of the surface fouling were detected by scanning electron microscopy and energy-dispersive X-ray spectrometer to identify the fouling crystal type. The results show that the titanium tube surface has a better anti-fouling performance compared with aluminum-brass tube. The mass increment of fouling deposition does not show a positive correlation with calcium ion concentration, rather it is influenced by the presence of magnesium ions and the type of surface material. We also found that the magnesium-to-calcium ion concentration ratio largely affects the fouling deposition, therefore, adding a certain proportion of magnesium ions to the solution can effectively reduce the fouling.

Keywords: Fouling deposition; Magnesium-to-calcium ion concentration ratio; Aluminum-brass tube; Titanium tube; Crystallization

1. Introduction

Fouling as the accumulation of salt crystal deposited on the liquid–solid surface is a ubiquitous phenomenon in numerous industrial fields, such as thermal desalination [1–3], wastewater treatment [4,5], highly-salty chemical engineering [6–8]. Fouling on metal surface can largely increase the thermal resistance and influence the flow field, which reduces the heat transfer performance, system efficiency and equipment service life [3]. The type of fouling substance typically found on heated surfaces depends on the fluid passing through that surface. In thermal seawater desalination, typical fouling substances comprise calcium carbonate, magnesium hydroxide and calcium sulfate. Factors that affect fouling deposition include tube material, ion concentration, temperature, surface roughness and surface energy etc. [1,2,9–11].

Previous studies have investigated the fouling rate variation with the heat exchangers wall temperature. Alsadaie & Mujtaba [2] and Yang et al. [12] found the fouling rate increases with the surface temperature through the multi-stage flash desalination dynamic model and seawater fouling dynamic model. However, Ni et al. [13] pointed out that the fouling deposition increases with the increasing of salinity at 70°C, which differs from that at 80°C and 90°C.

The tube material significantly affects the crystallization of fouling. Teng et al. [14] experimentally investigated the fouling amount for several metal surface and obtained the order of anti- fouling performance, from the best to the worst, is stainless steel, brass, carbon steel, aluminum, and copper.

* Corresponding author.
† Co-corresponding author

Kazi et al. [15] also found the fouling amount on aluminum is larger than that on brass, and even larger than that on stainless steel. Furthermore, Oon et al. [16,17] demonstrated that the titanium coating on stainless steel heat exchanger surface can effectively decrease fouling. Al-Otaibi et al. [18] observed that the anti- fouling performance of coated carbon steel is better than that of titanium tube.

Several studies focused on the fouling evolution process, Kim et al. [19] divided $CaCO_3$ fouling process into three stages based on microscopic observation: induction stage, uniform generation stage of crystal nucleus and uniform growth stage of fouling. Mwaba et al. [20] conducted $CaSO_4$ crystallization experiments on a plate and observed that the crystal growth rate increases with the increasing of surface temperature. Moreover, either decreasing the fluid velocity or increasing the supersaturations can lead to the narrowing of induction period. Jiang et al. [21] showed that adding alkali to oilfield injection water can shorten the induction period of fouling nucleation and accelerate the formation of crystal nuclei.

$CaCO_3$ fouling crystallization can be mainly classified into three forms: aragonite, calcite and vaterite. Kitamura [22] studied the effect of Mg^{2+} ion on the precipitation of $CaCO_3$ crystals in $CaCl_2$ and Na_2CO_3 mixed brine. Their results showed that Mg^{2+} ion could be adsorbed on the surface of calcite, causing lattice distortion and promoting calcite crystallization. Shen et al. [23] experimentally studied the fouling morphology of aluminum-brass tube surface in 80°C brines with different concentrations of Mg^{2+} and Ca^{2+}. The results indicated that an appropriate amount of Mg^{2+} ion can induce $CaCO_3$ formation of scattered irregular crystals on the aluminum-brass tube surface. Peyghambarzadeh and Bahrami [24] stated that the fouling rate increases sharply with increasing calcium sulfate concentration based on Taguchi algorithm.

Surface roughness and surface energy also closely relatives to the fouling amount. Lei et al. [25] and Kazi et al. [26] found that the large surface roughness leads to the faster crystallization rate. Kazi et al. [26] and Jiang et al. [27] believed that the fouling on metal surface prefers to deposit on surfaces with larger surface energy.

Generally, although the phenomenon of fouling on metal surfaces has been extensively studied, research on fouling in low-temperature multiple-effect evaporators with the influence of Ca^{2+} and Mg^{2+} ion concentrations on fouling remains relatively limited. Therefore, a thorough investigation was conducted to analyze the influence of magnesium-to-calcium ion concentration ratio on the fouling morphology, as well as the comparison of fouling deposition between the aluminum-brass and titanium tube surfaces. This paper aims to pave the way for enhancement of anti-fouling in environment of low-temperature multi-effect distillation (MED) for desalination.

2. Apparatus and methods

Fig. 1 illustrates the schematic diagram of the experimental process. The test tubes with length of 20.0 mm, out-diameter of 25.4 mm and thickness of 0.7 mm were successively cleaned by ethanol and water prior to the experiments. The ion concentrations of the solution immersing the metal tube were determined by the ratios of the following six salts: NaCl, Na_2SO_4, $CaCl_2$, $MgSO_4$, $MgCl_2$, $NaHCO_3$, as listed in Table 1. The beakers containing tubes and typical solutions were placed into a thermostatic water bath with constant temperature of 70°C. The tubes were retrieved and weighed three times each 24 h. Prior to weighing, the tubes underwent dissolution and rinsing by deionized water in order to remove the soluble salts. Finally, the weight variations were measured by an electronic analytical balance. The whole immersion time was last for 63 h (not including measurement duration). After the experiments, the fouling on the tubes were observed and detected by scanning electron microscopy (SEM) and energy-dispersive X-ray spectroscopy. All the cases were carried out for no less than 3 times to ensure the repeatability.

The information of relevant apparatus and tube materials are listed in Tables 2 and 3, respectively. Titanium tubes and aluminum-brass tubes are applied in these experiments since they have been extensively used in horizontal tube falling film multi-effect-distillation for desalination with their good anti-corrosion and heat transfer performance [15,16].

3. Results and discussion

3.1. Comparison between aluminum-brass and titanium tubes

Fig. 2 shows the mass variation of fouling deposition on the aluminum-brass and titanium tubes with cases 4, 10 and 16 in Table 1. (Case 16 has a salinity of 10%, which

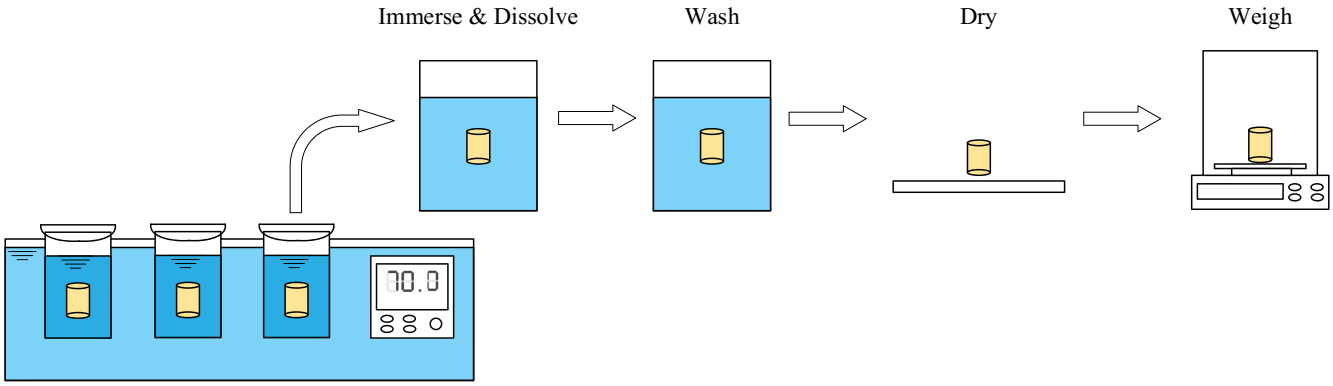

Fig. 1. Schematic diagram of experimental process.

Table 1
Ion concentrations

Case	Ca^{2+} (mol/L)	Mg^{2+} (mol/L)	Na^{+} (mol/L)	Cl^{-} (mol/L)	SO_4^{2-} (mol/L)	HCO_3^{-} (mol/L)
1	0.019	0.304	1.1331	1.610	0.081	0.0071
2		0.209	1.3231			
3		0.152	1.4371			
4		0.0912	1.5587			
5		0.0665	1.6081			
6		0	1.7411			
7	0.025	0.4	0.9291			
8		0.275	1.1791			
9		0.2	1.3291			
10		0.12	1.4891			
11		0.0875	1.5541			
12		0	1.7291			
13	0.032	0.512	0.6911			
14		0.352	1.0111			
15		0.256	1.2031			
16		0.154	1.4079			
17		0.112	1.4911			
18		0	1.7151			

Table 2
Experimental apparatus

Apparatus	Model	Accuracy
PH meter	PH838	0.01 pH
Electronic analytical balance	LICHEN FA224C	0.1 mg
Thermostat water bath	LICHEN LC-WB-6	0.1°C
Scanning electron microscopy	Quattro S	–
Energy disperse spectroscopy	Octane Elect	–

Table 3
Tube materials

Test tube	Material model	Ra (μm)	Surface energy (mJ/m²)
Aluminum-brass tube	HAl 77-2	0.579	20.56
Titanium tube	TA 1	0.571	18.64

is equivalent to the concentrated natural seawater used in this experiment). The fouling deposition on titanium tubes in the three cases were all smaller than that of aluminum-brass tubes. The mass of fouling deposition on the aluminum-brass tubes is approximately 2.04, 1.26 and 3.41 times larger than that on the titanium tube surface in cases 4, 10 and 16, respectively. The difference is caused by the two reasons: Firstly, the titanium surface has a lower surface energy, which means the fouling crystals are more difficult to be absorbed on the surface. Secondly, the titanium surface readily forms a denser titanium dioxide (TiO_2) layer compared with the aluminum oxide (Al_2O_3) layer of aluminum-brass surface [27].

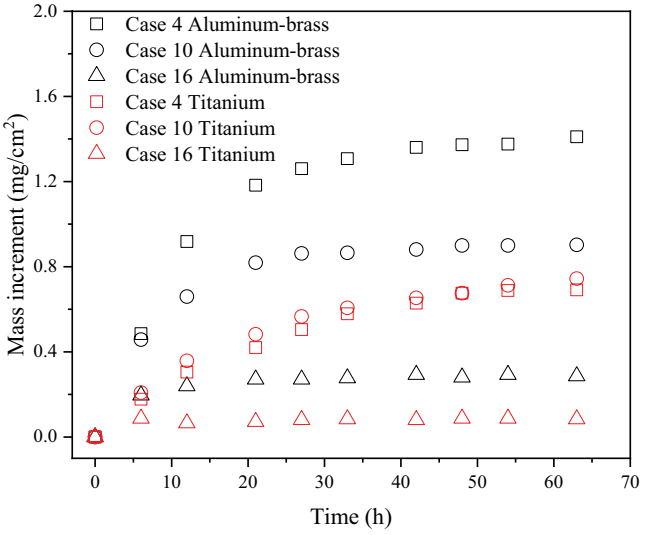

Fig. 2. Mass increment of fouling deposition for aluminum-brass and titanium tube.

The SEM images for case 16 of aluminum-brass and titanium tube are shown in Fig. 3, respectively. The crystal layer on aluminum-brass is continuous and thick since the $CaCO_3$ crystals are interconnected in the form of calcite forming cohesive crystalline structure. In some regions uncovered by the $CaCO_3$ calcite crystal layer, plate-like $Mg(OH)_2$ crystals can be observed.

Due to the supersaturation of $Mg(OH)_2$ crystal is lower than that of $CaCO_3$ crystal, $Mg(OH)_2$ crystal preferentially grows on the metal surface. Then, the $CaCO_3$ crystals are adsorbed on the $Mg(OH)_2$ crystal surface, thereby facilitating the $Mg(OH)_2$ agglomeration. The synergistic deposition

of both two crystals has resulted in a substantial increase in fouling on the aluminum-brass tube surface. To be greatly differ from aluminum-brass surface, the $CaCO_3$ crystals distributes dispersedly and discontinuously on the titanium tube surface, however, no other crystal forms can be observed. Attributed to the low surface energy of the titanium tube, both $Mg(OH)_2$ and $CaCO_3$ exhibit limited deposition on the surface of the titanium tube. Obviously, the titanium tube surface has a better anti-fouling performance compared with aluminum-brass surfaces.

3.2. Effect of calcium ion concentration

The comparison of cases 6, 12 and 18 aims to examine the influence of Ca^{2+} ion concentration on the fouling deposition without Mg^{2+}. The cases of 4, 10 and 16 have the same magnesium-to-calcium ion concentration ratio, which are used to obtain the influence of calcium ion concentration on fouling in the presence of Mg^{2+}.

3.2.1. Comparison without magnesium ion

The fouling deposition does not always increase with Ca^{2+} ion concentration, as shown in Fig. 4. Fig. 4a indicates the Ca^{2+} ion concentration of 0.032 mol/L has the largest 63-h mass increment of fouling deposition on aluminum-brass tube (nearly reaches to 0.6 mg/cm^2). Combined with Fig. 5c, the aluminum-brass surface with Ca^{2+} ion concentration of 0.032 mol/L has smaller crystals, but these small-sized crystals form a thicker and denser crystal layer. In the interstices of the crystal layers in Fig. 5c, tiny calcite calcium carbonate, acicular anatase-type calcium carbonate and spherulitic calcium carbonate are observed. At a calcium ion concentration of 0.025 mol/L, the crystal layer thickness is thinnest among these three concentrations and a considerable amount of smaller spherulitic calcite can be observed in the interstices, as shown in Fig. 5b, with the minimum 63-h mass increment. The crystal layer thickness with concentration of 0.019 mol/L is between that of 0.025 and 0.032 mol/L, as does the corresponding mass increment.

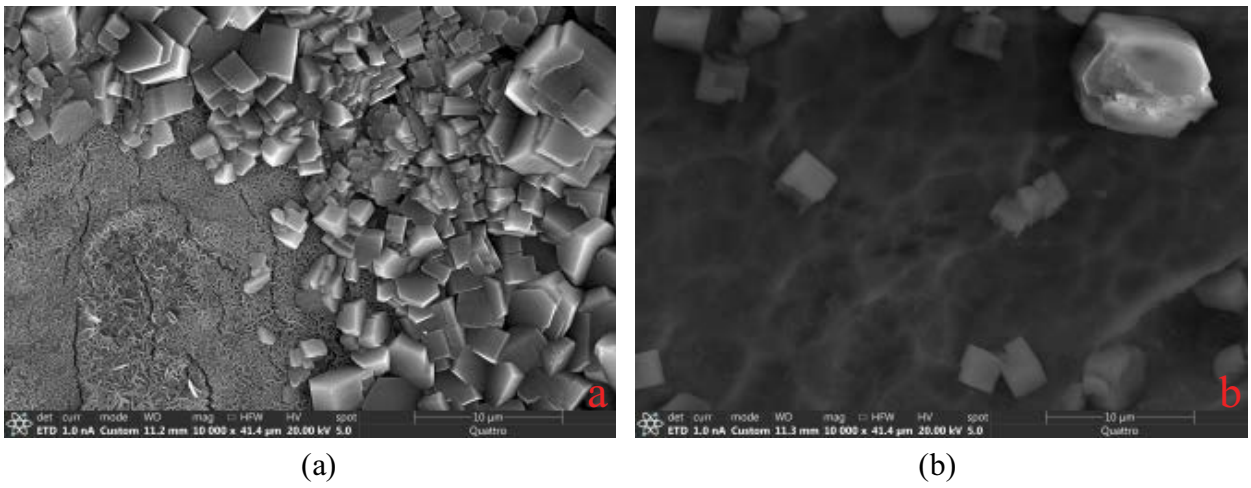

Fig. 3. Scanning electron microscopy images of fouling on (a) aluminum-brass and (b) titanium tube (case 16).

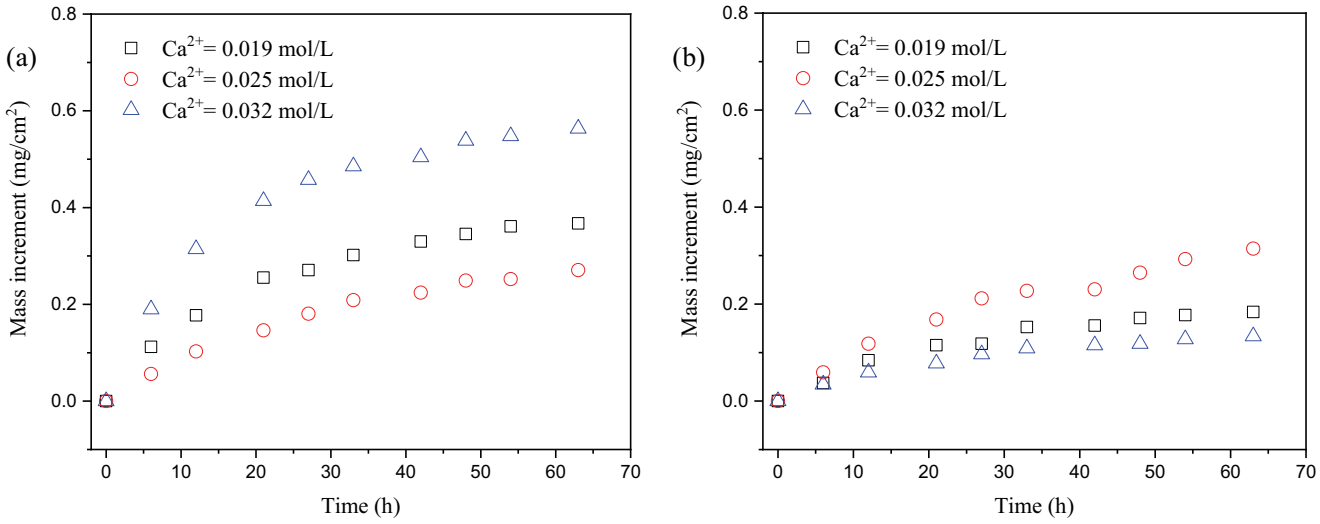

Fig. 4. Effect of calcium ion concentration without Mg^{2+} ion (a) aluminum-brass tube (b) titanium tube.

Unlike aluminum brass tubes, the calcium carbonate crystals on the surface of titanium tubes have not formed continuous crystal layers and the predominant crystal structure is calcite in all three concentrations. Their morphologies are quite similar, as shown in Fig. 5d–f. The crystal distribution density at 0.025 mol/L is slightly higher than the other two, resulting in a slightly greater mass increment of fouling deposition, as shown in Fig. 4b.

In conclusion, the influence of calcium ion concentration on fouling deposition is highly complex, which involves surface type and participant ions. Ultimately, the mass increment of fouling deposition dominated by crystal size, crystal type, crystal distribution density and crystal layer thickness.

3.2.2. Comparison with same magnesium-to-calcium ion concentration ratio

Fig. 6 illustrates that the fouling deposition on the surface of aluminum-brass and titanium tubes generally decreases with the Ca^{2+} ion concentration when magnesium-to-calcium ion concentration ratio R is 4.8. As for titanium tube, the difference between Ca^{2+} ion concentration 0.019 and 0.025 mol/L is marginal.

At calcium ion concentration of 0.019 mol/L, the calcium carbonate calcite crystals on aluminum-brass surface are larger and more regular. However, the crystal size slightly decreases when the concentration is 0.025 mol/L. While calcium ion concentration reaches 0.032 mol/L, the fouling

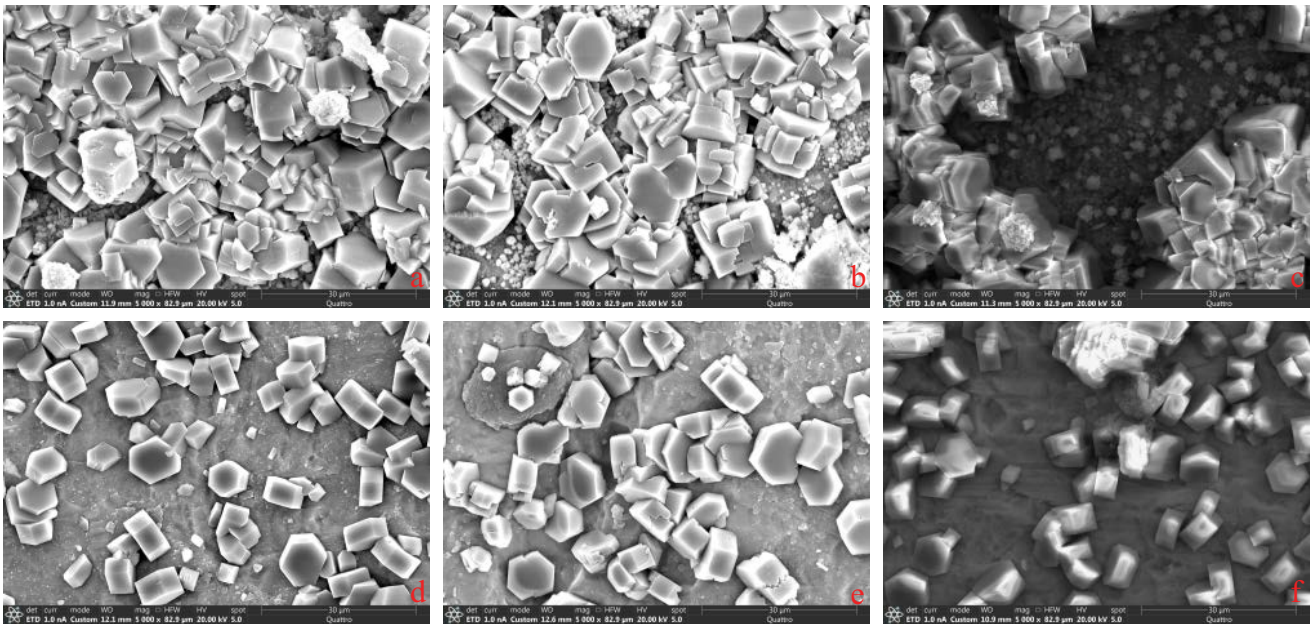

Fig. 5. Scanning electron microscopy images of fouling on aluminum-brass tube without Mg^{2+} ion (a) Ca^{2+} = 0.019 mol/L, (b) Ca^{2+} = 0.025 mol/L, (c) Ca^{2+} = 0.032 mol/L and titanium tube (d) Ca^{2+} = 0.019 mol/L, (e) Ca^{2+} = 0.025 mol/L, and (f) Ca^{2+} = 0.032 mol/L.

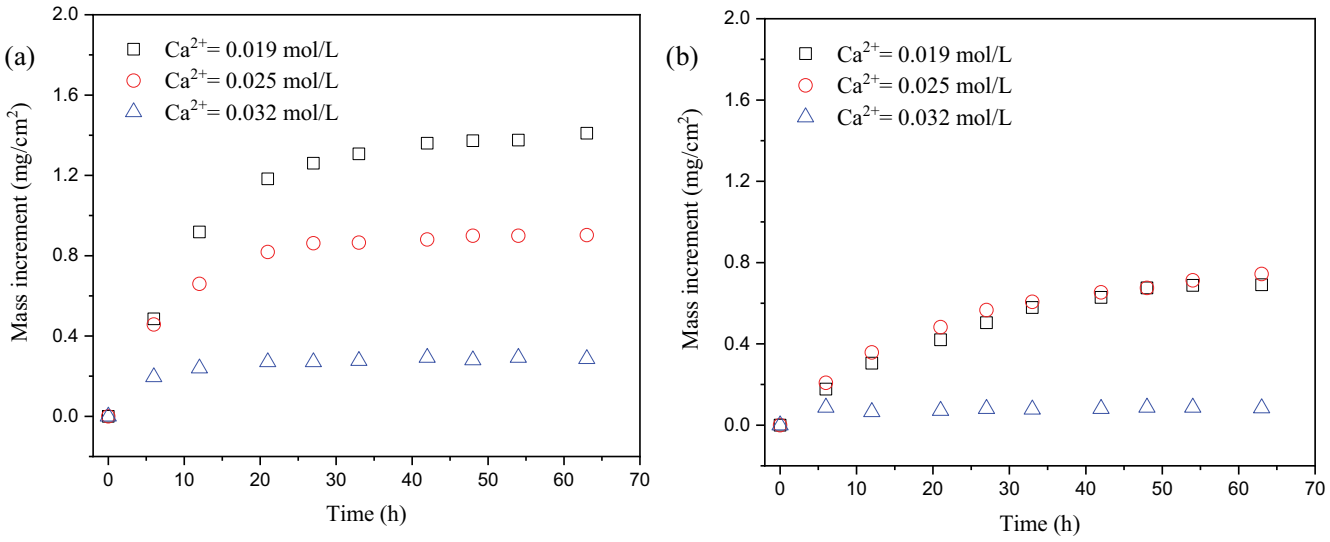

Fig. 6. Effect of calcium ion concentration with same R (a) aluminum-brass tube and (b) titanium tube.

shows continuous, irregular and smaller-sized calcite crystals, as shown in Fig. 7a–c. The crystal form on titanium surface under the concentration of 0.019 mol/L also shows a larger size and more regular morphology but no small calcite crystals are observed. Similarly, the crystal with the concentration of 0.025 mol/L has a slightly smaller size but accompanying calcite crystals. This might account for the relatively minor differences observed between 0.019 and 0.025 mol/L. However, at a calcium ion concentration of 0.032 mol/L, the fouling on titanium surface exhibits discontinuous, small-sized calcite crystals.

As the concentration of calcium ions increases, there is an unexpected decrease in the fouling formation. This phenomenon can be attributed to the rising magnesium ion concentration although the magnesium-to-calcium ion concentration ratio remain the same. Evidently, the absolute concentration of magnesium ions exerts an inhibitory effect on the fouling. Magnesium ions influence the calcium carbonate crystallization, particularly the calcite growth rate, leading to the generation of distinct crystal types [28–31]. Mg^{2+} inhibits regular calcite growth by incorporating into the $CaCO_3$ lattice since Mg^{2+} ions partially replace Ca^{2+} ions and occupy the lattice positions necessary for the normal growth of crystals [32,33]. The instable $CaCO_3$ crystals with Mg^{2+} ions embedded exhibit internal stresses. Consequently, cracks and fractures are developed in the crystals, leading to splitting into small, cracked calcite, as shown in Fig. 7f.

In a word, due to the significant increase in magnesium ions, which enhances the probability of occupying calcium ion sites, it induces lattice distortion in calcium carbonate crystals, resulting in irregular crystallization and reduces fouling deposition.

Table 4
Cases with different *R*

Case	*R*
6,12,18	0
5,11,17	3.5
4,10,16	4.8
3,9,15	8
2,8,14	11
1,7,13	16

3.3. Effect of magnesium-to-calcium ion concentration ratio

According to Section 3.2 – Effect of calcium ion concentration, appropriate concentrations of Mg^{2+} ion can reduce the fouling deposition on aluminum-brass and titanium surface. Therefore, in this section, the effects of 6 different magnesium-to-calcium ion concentration ratios on the fouling deposition were performed based on three calcium ion concentrations, as listed in Table 4. In order to minimize the influence of different ion strengths on the fouling deposition, solutions with similar ion strengths were used in the experimental tests. The ion strength *I* calculated by Eq. (1):

$$I = \frac{1}{2}\sum mz^2 \tag{1}$$

where *m* refers to the mass molar concentration and *z* represents the valence.

Fig. 8 shows the effects of magnesium-to-calcium ion concentration ratio on 63-h mass increment of fouling deposition with different Ca^{2+} ion concentrations. According to Fig. 8a, it can be observed that the cumulative fouling deposition of Ca^{2+} ion concentration ratio 0.019 and 0.025 mol/L shows a trend of initially increasing and then

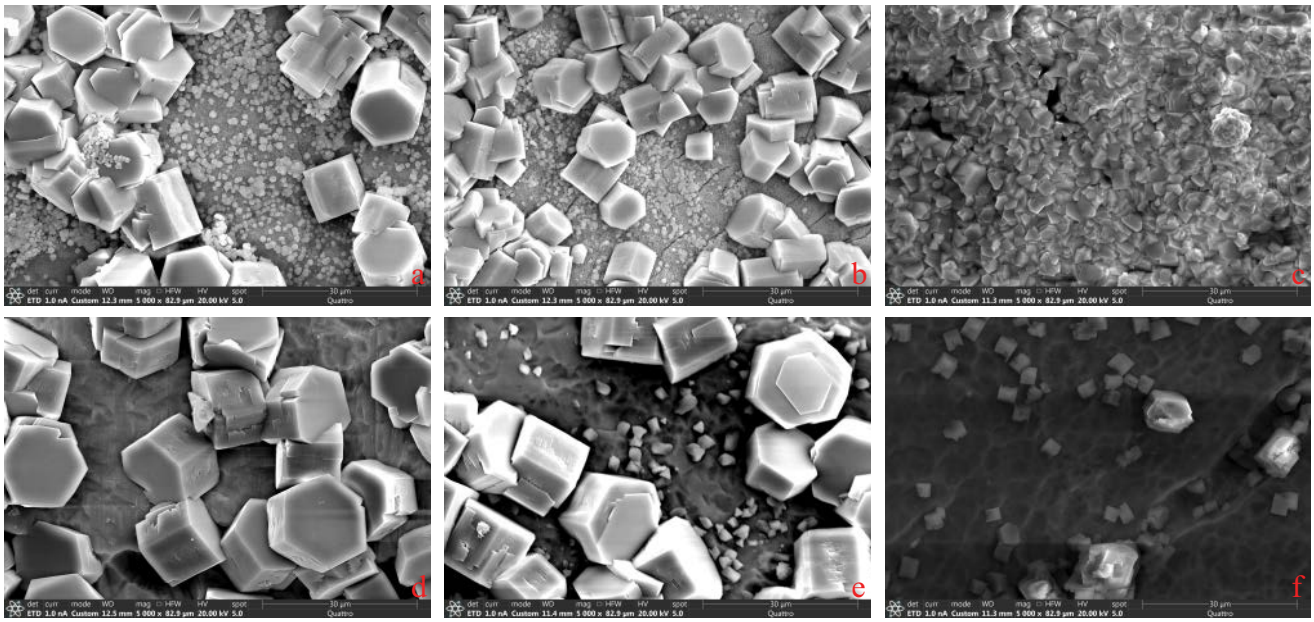

Fig. 7. Scanning electron microscopy images of fouling on aluminum-brass tube (a) Ca^{2+} = 0.019 mol/L, (b) Ca^{2+} = 0.025 mol/L, (c) Ca^{2+} = 0.032 mol/L and titanium tube (d) Ca^{2+} = 0.019 mol/L, (e) Ca^{2+} = 0.025 mol/L, and (f) Ca^{2+} = 0.032 mol/L.

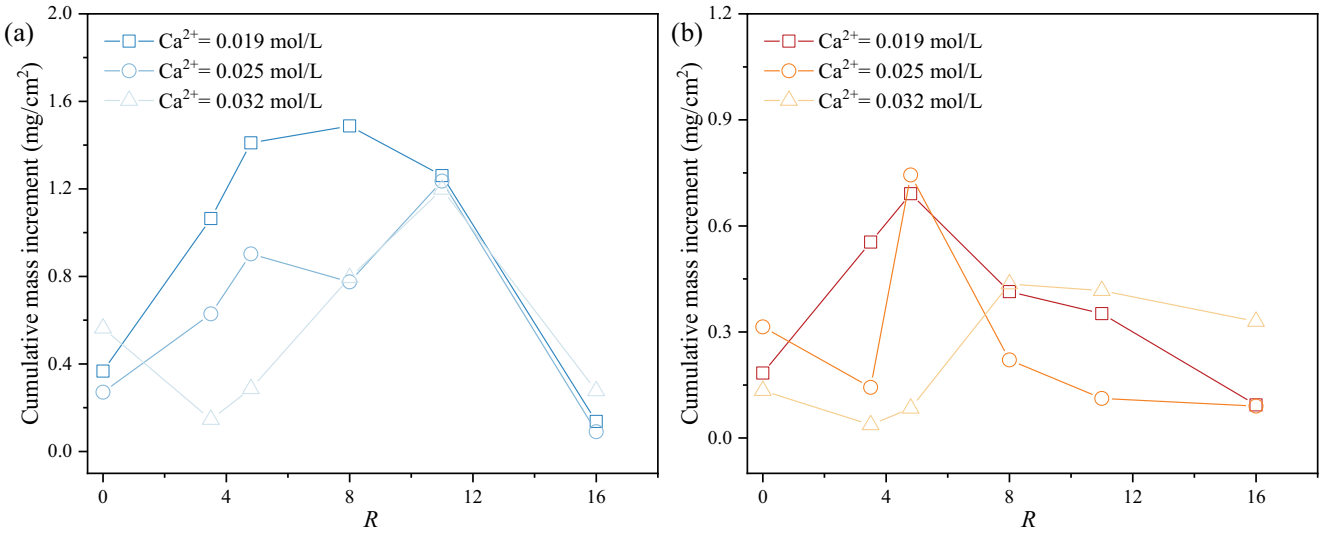

Fig. 8. Effects of magnesium-to-calcium ion concentration ratio (a) aluminum-brass tube and (b) titanium tube.

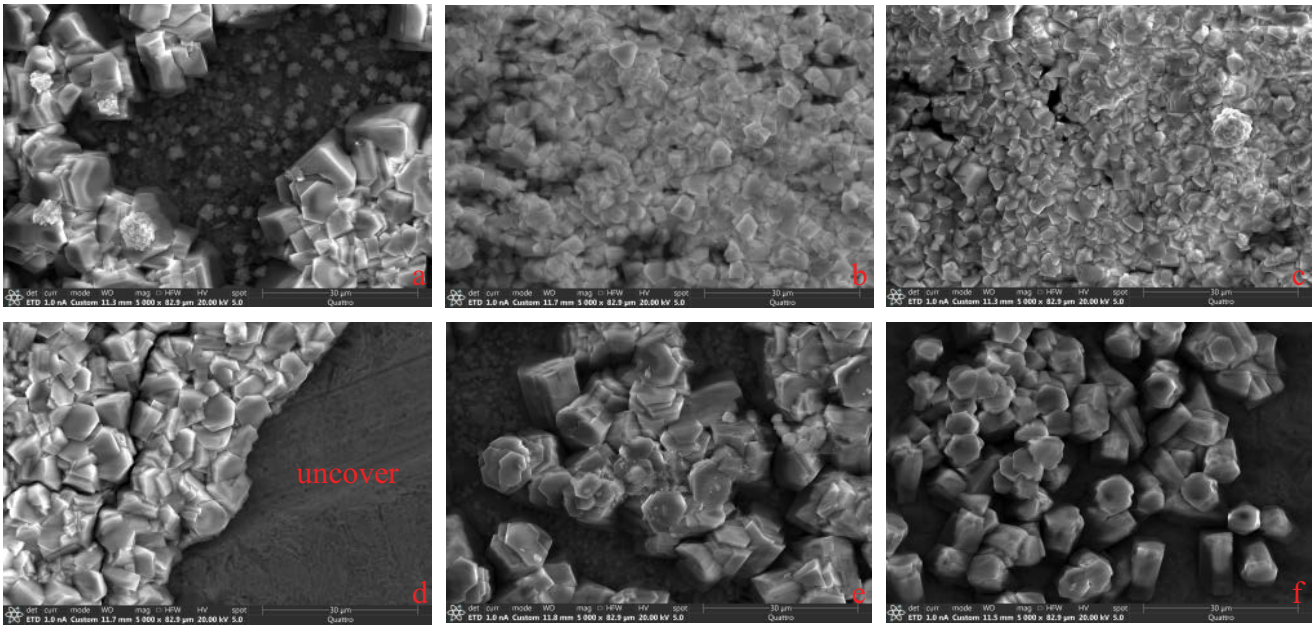

Fig. 9. Scanning electron microscopy images of fouling on aluminum-brass tube with different R at Ca^{2+} ion concentration of 0.032 mol/L (a) R = 0, (b) R = 3.5, (c) R = 4.8, (d) R = 8, (e) R = 11, and (f) R = 16.

decreasing with the increasing R. In our experimental range, the cumulative fouling deposition on the aluminum-brass tube surface is minimized at R = 16 and maximized round R = 8~12. Similarly, the minimum cumulative fouling deposition on the titanium tube surface with Ca^{2+} ion concentration of 0.019 and 0.025 mol/L is observed at R = 16, while that reach the maximum at R = 4.8, as shown in Fig. 8b.

For both titanium and aluminum-brass tubes at a Ca^{2+} ion concentration of 0.032 mol/L, the fouling deposition experiences two reductions with increasing of R in this experimental range. Combining Figs. 9 and 10, it can be observed that the first reduction appears at around R = 3.5~4.8 due to a decrease in the number of large-sized crystals and an increase in small-sized crystals. Subsequently, the second drop occurs at R approaching 16 since crystals became even more sparse and discontinuous.

Therefore, the addition of Mg^{2+} ions can obviously reduce the fouling deposition on both the aluminum-brass tube surface and titanium tube surface and obtain the corresponding crystal form. In conjunction with Section 3.2.2 – Comparison with same magnesium-to-calcium ion concentration ratio, it is also found that the significant fouling inhibition occurs only when the absolute Mg^{2+} ion concentration reaches a certain threshold.

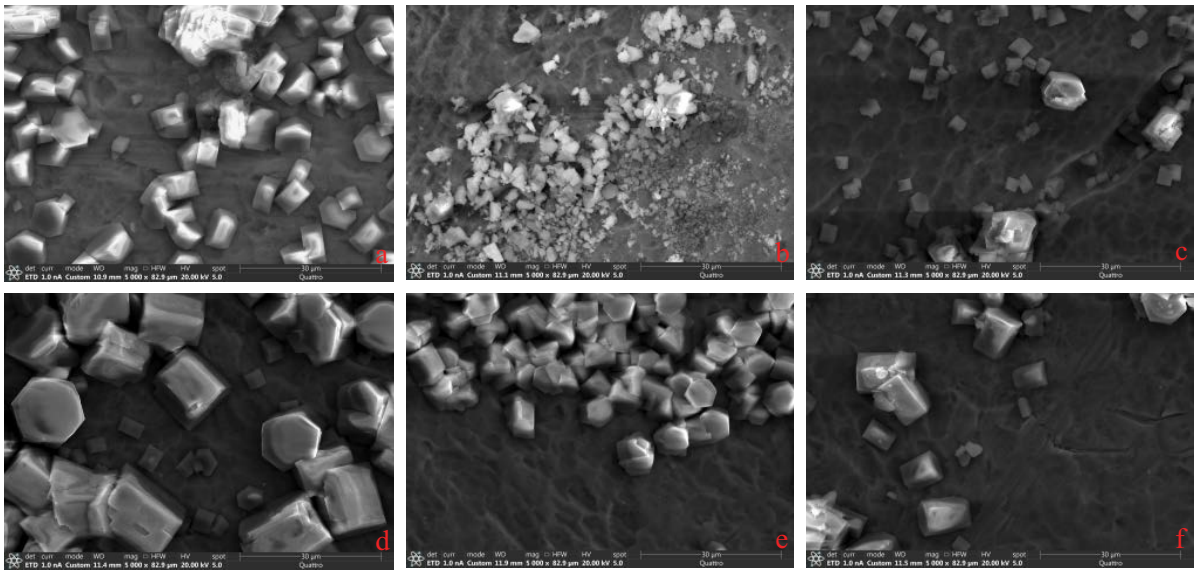

Fig. 10. Scanning electron microscopy images of fouling on titanium tube with different R at Ca^{2+} ion concentration of 0.032 mol/L (a) R = 0, (b) R = 3.5, (c) R = 4.8, (d) R = 8, (e) R = 11, and (f) R = 16.

4. Conclusions

In this work, the effects of calcium ion concentration and magnesium-to-calcium ion ratio on the fouling deposition and crystal morphology have been investigated on aluminum-brass tube and titanium tube in the environment of MED desalination. The results of this experiment demonstrate the fouling crystal types on the surfaces of aluminum-brass and titanium tubes in the MED environment under various conditions, providing references for effective fouling removal in subsequent stage. Additionally, the study illustrates that different magnesium-to-calcium ion ratios have a significant impact on the crystal morphology and quality of fouling, therefore offering a strategy for fouling inhibition in MED desalination. The conclusions are summarized as follows:

- The titanium tube surface is less prone to the formation of continuous crystals. Thus, it exhibits better performance in anti-fouling compared to aluminum brass.
- The mass increment of fouling deposition does not show a positive correlation with calcium ion concentration. It also depends on the presence of magnesium ions and the type of surface material.
- Under constant calcium ion concentration, the addition of a certain amount of magnesium ions can effectively reduce the fouling deposition.

Acknowledgement

The authors all wish to acknowledge Dr. Bo Qi for his helpful discussion on crystal formation.

References

[1] A. Stärk, K. Krömer, K. Loisel, K. Odiot, S. Nied, H. Glade, Impact of tube surface properties on crystallization fouling in falling film evaporators for seawater desalination, Heat Transfer Eng., 38 (2017) 762–774.
[2] S.M. Alsadaie, I.M. Mujtaba, Dynamic modelling of heat exchanger fouling in multistage flash (MSF) desalination, Desalination, 409 (2017) 47–65.
[3] T.R. Bott, Fouling of Heat Exchangers, Elsevier Science, Amsterdam, The Netherlands, 1995.
[4] A. Al-Gailani, O. Sanni, T.V.J. Charpentier, R. Barker, R. Crisp, H.J. Bruins, A. Neville, Role of temperature, roughness and pressure in crystallization fouling from potable water on aluminum surface, Therm. Sci. Eng. Prog., 23 (2021) 100911, doi: 10.1016/j.tsep.2021.100911.
[5] A. Deshmukh, C. Boo, V. Karanikola, S. Lin, A.P. Straub, T. Tong, D.M. Warsinger, M. Elimelech, Membrane distillation at the water-energy nexus: limits, opportunities, and challenges, Energy Environ. Sci., 11 (2018) 1177–1196.
[6] N. Andritsos, A.J. Karabelas, Calcium carbonate scaling in a plate heat exchanger in the presence of particles, Int. J. Heat Mass Transfer, 46 (2003) 4613–4627.
[7] K.S. Song, J. Lim, S. Yun, S. Yun, D. Kim, Y. Kim, Composite fouling characteristics of $CaCO_3$ and $CaSO_4$ in plate heat exchangers at various operating and geometric conditions, Int. J. Heat Mass Transfer, 136 (2019) 555–562.
[8] A. Vosough, M.R. Assari, S.M. Peyghambarzadeh, S. Azizi, Influence of fluid flow rate on the fouling resistance of calcium sulfate aqueous brine in subcooled flow boiling condition, Int. J. Therm. Sci., 154 (2020) 106397, doi: 10.1016/j.ijthermalsci.2020.106397.
[9] S. Hatte, R. Stoddard, R. Pitchumani, Generalized analysis of dynamic flow fouling on heat transfer surfaces, Int. J. Heat Mass Transfer, 188 (2022) 122573, doi: 10.1016/j.ijheatmasstransfer.2022.122573.
[10] K. Al-Anezi, N. Hilal, Scale formation in desalination plants: effect of carbon dioxide solubility, Desalination, 204 (2007) 385–402.
[11] M.A.K. Al-Sofi, Fouling phenomena in multi stage flash (MSF) distillers, Desalination, 126 (1999) 61–76.
[12] D.Z. Yang, J.H. Liu, X.X. E, L.L. Jiang, Model for seawater fouling and effects of temperature, flow velocity and surface free energy on seawater fouling, Chin. J. Chem. Eng., 24 (2016) 658–664.
[13] B. Ni, S.Q. Shen, X.H. Liu, S. Chen, Effects of temperature and salinity on fouling in hypersaline seawater, Desal. Water Treat., 173 (2020) 41–48.
[14] K.H. Teng, S.N. Kazi, A. Amiri, A.F. Habali, M.A. Bakar, B.T. Chew, A. Al-Shamma'a, A. Shaw, K.H. Solangi, G. Khan,

Calcium carbonate fouling on double-tube heat exchanger with different heat exchanging surfaces, Powder Technol., 315 (2017) 216–226.
[15] S.N. Kazi, K.H. Teng, M.S. Zakaria, E. Sadeghinezhad, M.A. Bakar, Study of mineral fouling mitigation on heat exchanger surface, Desalination, 367 (2015) 248–254.
[16] C.S. Oon, S.N. Kazi, M.A. Hakimin, A.H. Abdelrazek, A.R. Mallah, F.W. Low, S.K. Tiong, I.A. Badruddin, S. Kamanger, Heat transfer and fouling deposition investigation on the titanium coated heat exchanger surface. Powder Technol., 373 (2020) 671–680.
[17] C.S. Oon, S.N. Kazi, N. Zubir, I.A. Badruddin, S. Kamangar, C.Y. Heah, F. Alnaimat, B. Mathew, A. Husain, Fouling and fouling mitigation of mineral salt using bio-based functionalized graphene nano-plates, J. Therm. Anal. Calorim., 146 (2021) 265–275.
[18] D.A. Al-Otaibi, M.S.J. Hashmi, B.S. Yilbas, Fouling resistance of brackish water: comparison of fouling characteristics of coated carbon steel and titanium tubes, Exp. Therm. Fluid Sci., 55 (2014) 158–165.
[19] W.T. Kim, C. Bai, Y.I. Cho, A study of $CaCO_3$ fouling with a microscopic imaging technique, Int. J. Heat Mass Transfer, 45 (2002) 597–607.
[20] M.G. Mwaba, C.C.M. Rindt, A.A. van Steenhoven, M.A.G. Vorstman, Experimental investigation of $CaSO_4$ crystallization on a flat plate, Heat Transfer Eng., 27 (2006) 42–54.
[21] H.Y. Jiang, H.H. Cai, A.G. Liang, D.Z. Zhang, N.N. Sun, X.M. Chong, Effect of alkali about growth characteristics of $CaCO_3$ on galvanized iron surface, CIESC J., 70 (2019) 170–178 (in Chinese).
[22] M. Kitamura, Crystallization and transformation mechanism of calcium carbonate polymorphs and the effect of magnesium ion, J. Colloid Interface Sci., 236(2001) 318–327.
[23] S.Q. Shen, B. Ni, Y.H. Li, X.H. Liu, The effects of Ca^{2+} and Mg^{2+} ion concentrations in brine on scaling formation and morphology on metal surfaces, Desal. Water Treat., 221 (2021) 11–22.
[24] S.M. Peyghambarzadeh, N. Bahrami, Statistical analysis of calcium sulfate scaling under boiling heat transfer, Appl. Therm. Eng., 53 (2013) 108–113.
[25] C.W. Lei, Z.X. Peng, T. Day, X.P. Yan, X.Q. Bai, C.Q. Yuan, Experimental observation of surface morphology effect on crystallization fouling in plate heat exchangers, Int. Commun. Heat Mass Transfer, 38 (2011) 25–30.
[26] S.N. Kazi, G.G. Duffy, X.D. Chen, Fouling and fouling mitigation on heated metal surfaces, Desalination, 288 (2012) 126–134.
[27] H.Y. Jiang, D.Z. Zhang, A.G. Liang, H.H. Cai, N.N. Sun, X.M. Zhong, Effect mechanism of material type on crystallization growth of $CaCO_3$-based scale, Surf. Technol., 47 (2018) 255–262 (in Chinese).
[28] M. Deleuze, S.L. Brantley, Inhibition of calcite crystal growth by Mg^{2+} at 100°C and 100 bars: influence of growth regime, Geochim. Cosmochim. Acta, 61 (1997) 1475–1485.
[29] J.D. Rodriguez-Blanco, S. Shaw, P. Bots, T. Roncal-Herrero, L.G. Benning, The role of Mg in the crystallization of monohydrocalcite, Geochim. Cosmochim. Acta, 127 (2014) 204–220.
[30] J.W. Morse, A. Mucci, L.M. Walter, Magnesium interaction with the surface of calcite in seawater, Science, 205 (1979) 904–905.
[31] A.E.S. van Driessche, M. Kellermeier, L.G. Benning, D. Gebauer, New Perspectives on Mineral Nucleation and Growth: From Solution Precursors to Solid Materials, Springer, Switzerland, 2017.
[32] K.J. Davis, P.M. Dove, J.J. De Yoreo, The role of Mg^{2+} as an impurity in calcite growth, Science, 290 (2000) 1134–1137.
[33] A. Mucci, J.W. Morse, The incorporation of Mg^{2+} and Sr^{2+} into calcite overgrowths: influences of growth rate and solution composition, Geochim. Cosmochim. Acta, 47(1983) 217–233.